background, SHR generated additional ground tissue layers, as previously described (*7*, *9*). However, when expressed in combinations of mutants involving *blj jkd* and *scr*, SHR failed to rescue the formative cell divisions within the ground tissue. These results indicate that BLJ, JKD, and SCR are essential for SHR to carry out ground tissue patterning. Furthermore, analysis of the contribution of the BIRDs and SCR to generate specific gene expression patterns showed that these transcription factors were able to activate expression of endodermis and cortex genes (Fig. 4C). Staining for endodermis-specific attributes (the Casparian strip) in the *shr* J0571xUAS lines showed that BLJ (Fig. 4, D to F), along with the other BIRDs and SCR (fig. S7, M to Q), could induce Casparian strip formation subsequent to periclinal divisions of the ground tissue. Expression of cortex-specific markers required at least JKD, MGP, and NUC (Fig. 4, G and H). SCZ, which is required for expression of some cortex-specific markers (*15*), is also a target in the network. Our analysis suggests that cortex identity requires multiple inputs from the BIRDs. Therefore, the BIRDs and SCR, in addition to mediating SHR transcriptional competence (*7*), are endogenous effectors of ground tissue patterning and can provide all the necessary information for the asymmetric divisions that are activated by SHR to pattern the ground tissue.

Cell fate choices in all multicellular organisms are governed by transcription factors. Their combinatorial expression and interactions are key to tissue identity. The BIRDs and SCR play critical roles in maintaining ground tissue identity in postembryonic roots by specifying the CEI stem cells that generate the ground tissue lineage (Fig. 4I). In addition, they are effectors of asymmetric divisions that pattern the progeny of the CEIs (Fig. 4J). The continuous control of multiple steps of tissue formation by the same set of transcription factors, independently of and dependent on positional cues, is a sophisticated mechanism ensuring plasticity in the regulation of cell fate.

REFERENCES AND NOTES

1. J. J. Petricka, J. M. Van Norman, P. N. Benfey, *Cold Spring Harb. Perspect. Biol.* **1**, a000497 (2009).
2. D. Welch *et al.*, *Genes Dev.* **21**, 2196–2204 (2007).
3. H. Cui *et al.*, *Science* **316**, 421–425 (2007).
4. A. Cruz-Ramírez *et al.*, *Cell* **150**, 1002–1015 (2012).
5. R. Sozzani *et al.*, *Nature* **466**, 128–132 (2010).
6. M. P. Levesque *et al.*, *PLOS Biol.* **4**, e143 (2006).
7. Y. Long *et al.*, *Plant Cell* **27**, 1185–1199 (2015).
8. R. Zhou, L. M. Benavente, A. N. Stepanova, J. M. Alonso, *Plant J.* **66**, 712–723 (2011).
9. Y. Helariutta *et al.*, *Cell* **101**, 555–567 (2000).
10. M. Pernas, E. Ryan, L. Dolan, *Curr. Biol.* **20**, 818–823 (2010).
11. M. Aida *et al.*, *Cell* **119**, 109–120 (2004).
12. V. Willemsen *et al.*, *Dev. Cell* **15**, 913–922 (2008).
13. Materials and methods are available as supplementary materials on *Science* Online.
14. S. M. Brady *et al.*, *Science* **318**, 801–806 (2007).
15. C. A. ten Hove *et al.*, *Curr. Biol.* **20**, 452–457 (2010).

ACKNOWLEDGMENTS

This work was supported by grants from the NIH (R01-GM043778) and the Gordon and Betty Moore Foundation (GBMF3405) to P.N.B.; from the NSF (IOS-1021619-002) to U.O. and P.N.B.; and from MINECO, FEDER/EFDR (BFU2013-41160-P), and FP7 (PCIG11-GA-2012-322082) to M.A.M.-R. M.A.M.-R is supported by the Ramon y Cajal program (MINECO), C.M.W. by a NRSA F32 GM106690-01 fellowship, I.B. by a NWO VIDI grant, and B.S. by an ERC Advanced Grant SysArc. J.J.P. was supported by a NIH Ruth L. Kirschstein NRSA F32 GM086976 fellowship I.B. by a NWO VIDI grant, and B.S. by an ERC Advanced Grant SysArc. We thank D. R. McClay, D. M. Pernas, and Y. Long for critical reading of the manuscript. Additional data are in the supplementary materials. The National Center for Biotechnology Information Gene Expression Omnibus accession numbers are GSE60157 (microarrays) and GSE60011 (ChIP-Seq). The authors declare that they have no competing interests.

SUPPLEMENTARY MATERIALS

www.sciencemag.org/content/350/6259/426/suppl/DC1
Materials and Methods
Figs. S1 to S7
Table S1 to S6
References (*16*–*30*)

30 July 2015; accepted 22 September 2015
10.1126/science.aad1171

ALZHEIMER'S DISEASE

Reduced grid-cell–like representations in adults at genetic risk for Alzheimer's disease

Lukas Kunz,[1,2] Tobias Navarro Schröder,[3] Hweeling Lee,[1] Christian Montag,[4] Bernd Lachmann,[4] Rayna Sariyska,[4] Martin Reuter,[5,6] Rüdiger Stirnberg,[1] Tony Stöcker,[1] Paul Christian Messing-Floeter,[1,2] Juergen Fell,[2] Christian F. Doeller,[3]* Nikolai Axmacher[1,2,7]*†

Alzheimer's disease (AD) manifests with memory loss and spatial disorientation. AD pathology starts in the entorhinal cortex, making it likely that local neural correlates of spatial navigation, particularly grid cells, are impaired. Grid-cell–like representations in humans can be measured using functional magnetic resonance imaging. We found that young adults at genetic risk for AD (*APOE*-ε4 carriers) exhibit reduced grid-cell–like representations and altered navigational behavior in a virtual arena. Both changes were associated with impaired spatial memory performance. Reduced grid-cell–like representations were also related to increased hippocampal activity, potentially reflecting compensatory mechanisms that prevent overt spatial memory impairment in *APOE*-ε4 carriers. Our results provide evidence of behaviorally relevant entorhinal dysfunction in humans at genetic risk for AD, decades before potential disease onset.

Late-onset AD is the most common form of dementia and one of the most challenging diseases of modern society (*1*). Curative therapies are still lacking, presumably because they start too late (*2*). Therefore, the elucidation of early pathomechanisms underlying symptoms of AD is of high interest. We aimed at identifying one of the potentially earliest neurocognitive pathomechanisms in the development of AD symptoms: We hypothesized entorhinal dysfunction in young *APOE*-ε4 carriers. Our hypothesis was built on three previous findings: First, the ε4 allele of the *APOE* gene is the strongest genetic risk factor for late-onset AD (*3*). Individuals carrying one *APOE*-ε4 allele are at threefold increased risk of AD, and those carrying two *APOE*-ε4 alleles are at more than 10-fold increased risk (*4*). Second, early AD histopathology appears in the entorhinal cortex (EC) (*5*), where tau abnormalities can already be observed in adults under the age of 30 (*6*), especially in *APOE*-ε4 carriers (*7*). Third, the EC contains grid cells, a cell type involved in spatial navigation. Grid cells fire whenever animals (*8*) or humans (*9*) traverse the vertices of an internally generated grid tiling the spatial environment into equilateral triangles. Their function has been linked to path integration (*10*, *11*), error correction (*12*), and the maintenance of place cells (*13*), which exhibit only a singular firing field (*14*). Hence, a possible dysfunction of grid cells may provide an explanation for the symptom of spatial disorientation in patients suffering from AD. Proxies for grid cells, termed grid-cell–like representations, are detectable in humans by functional magnetic resonance imaging (fMRI). The blood oxygenation level–dependent signal of the EC depends on movement direction with sixfold rotational symmetry. More specifically, the contrast of brain activity during movements aligned versus misaligned to the main axes of a putative grid in a virtual arena leads to a macroscopically visible fMRI signal in the right EC (*15*).

We examined the effect of *APOE*-ε4 on grid-cell–like representations by comparing two groups of healthy young adults (n = 38 *APOE*-ε4/ε3 carriers, termed "risk participants" from now on; n = 37 ε3/ε3 carriers, "control participants"; table S1). Participants completed a previously established

[1]German Center for Neurodegenerative Diseases (DZNE), Bonn, Germany. [2]Department of Epileptology, University of Bonn, Bonn, Germany. [3]Donders Institute for Brain, Cognition and Behaviour, Radboud University, Nijmegen, Netherlands. [4]Department of Psychology, Ulm University, Ulm, Germany. [5]Department of Psychology, University of Bonn, Bonn, Germany. [6]Center for Economics and Neuroscience, University of Bonn, Bonn, Germany. [7]Department of Neuropsychology, Institute of Cognitive Neuroscience, Ruhr-University Bochum, Bochum, Germany. *These authors contributed equally to this work. **†Corresponding author. E-mail: nikolai.axmacher@rub.de**

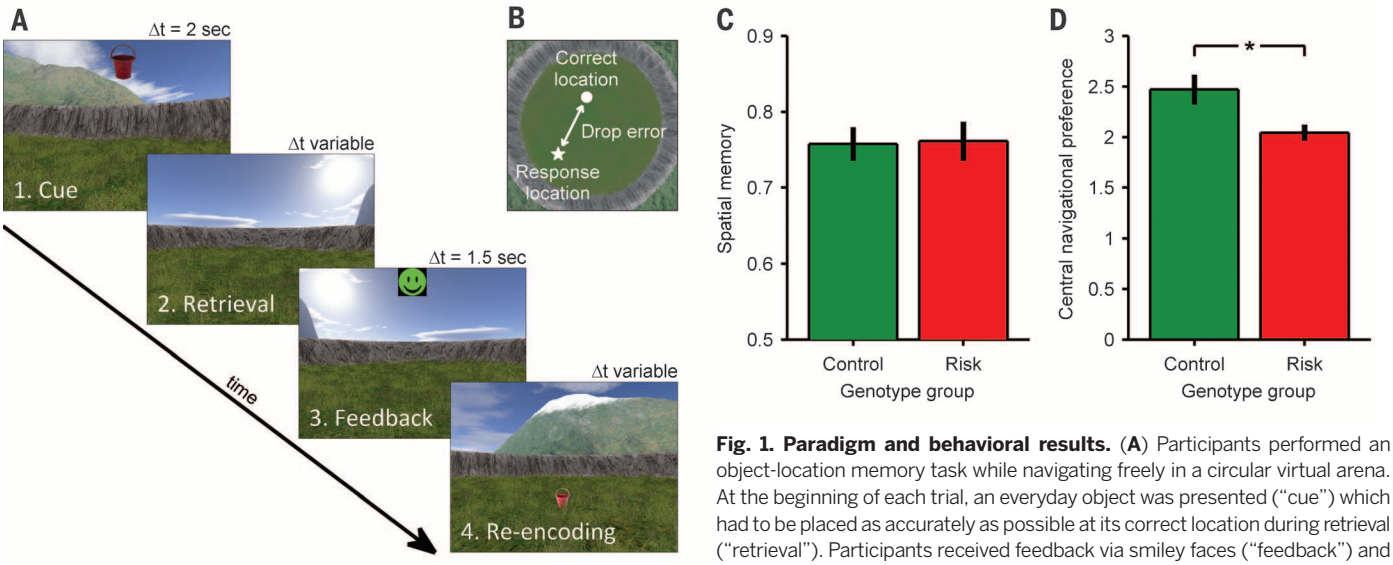

Fig. 1. Paradigm and behavioral results. (**A**) Participants performed an object-location memory task while navigating freely in a circular virtual arena. At the beginning of each trial, an everyday object was presented ("cue") which had to be placed as accurately as possible at its correct location during retrieval ("retrieval"). Participants received feedback via smiley faces ("feedback") and re-encoded the object position afterward ("re-encoding"). Δ*t*, time for specific trial phase. (**B**) For each participant, the drop error was calculated as the difference between response locations and correct locations averaged across trials. To improve readability, drop error values were transformed into spatial memory performance values (methods). (**C**) Spatial memory performance does not differ between control (*APOE*-ε3/ε3; $n = 37$) and risk (*APOE*-ε4/ε3; $n = 38$) participants. (**D**) Risk participants show a reduced preference to navigate within the arena center as compared to control participants. All bars show mean and standard error of the mean (SEM) across participants. *$P < 0.05$.

paradigm for the detection of grid-cell–like representations (*15*), during which they performed an object-location memory task while navigating freely in a virtual environment (Fig. 1 and figs. S1 and S2). Briefly, the analysis split the fMRI data into two halves (Fig. 2 and tables S4 and S5): The first half served to identify the angular orientation of the putative grid axes (separated by angles of 60°, which is equivalent to the sixfold rotational symmetry of the grid) relative to the environment in each participant's right EC (*16*). The second half of the data was then used to contrast brain activity during movements aligned with these grid axes versus brain activity during misaligned movements. The averaged contrast values of aligned versus misaligned movements across all voxels in the right EC reflect the magnitude of grid-cell–like representations [exemplary participant-specific EC region of interest (ROI); Fig. 2D]. We found significant grid-cell–like representations in control participants ($t_{36} = 2.318$, $P = 0.026$) but not in risk participants ($t_{37} = -1.730$, $P = 0.092$). In fact, the magnitude of grid-cell–like representations was strongly reduced in risk participants as compared to control participants [$t_{73} = 2.875$, $P = 0.005$; Fig. 2; two-way genotype × sex analysis of variance (ANOVA): main effect of genotype, $F_{1,71} = 8.695$, $P = 0.004$; no main effect of sex, $F_{1,71} = 0.709$, $P = 0.403$; no interaction, $F_{1,71} = 1.838$, $P = 0.179$]. Control analyses showed that our finding in control participants was specific for sixfold rotational symmetry and specific for the right EC (fig. S3). No structural changes of the right EC, which could potentially account for the functional changes, were observed (fig. S4).

In contrast to the genotype effect on grid-cell–like representations, both genetic subgroups showed similar spatial memory performance ($t_{73} = -0.109$, $P = 0.913$; Fig. 1) as well as similar basic behavioral characteristics (table S2). We assume that the detrimental effect of *APOE*-ε4 on spatial memory becomes apparent only at older age (*17*), when histopathological changes due to presymptomatic AD have reached adjacent limbic regions such as the hippocampus. However, risk participants exhibited altered navigational behavior. They showed a reduced preference to navigate in the center of the arena ("central navigational preference"; methods) as compared to control participants ($t_{73} = 2.551$, $P = 0.014$; Fig. 1 and fig. S1; two-way genotype × sex ANOVA: main effect of genotype, $F_{1,71} = 6.293$, $P = 0.014$; no main effect of sex, $F_{1,71} = 0.094$, $P = 0.761$; no interaction, $F_{1,71} = 1.978$, $P = 0.164$). This finding was also reflected in a greater mean distance of all virtual positions relative to the arena center in risk participants ($t_{73} = -3.003$, $P = 0.004$; fig. S5).

Next, we examined whether the *APOE*-dependent changes of grid-cell–like representations and central navigational preference were related to spatial memory performance. Using linear multiple regression (Table 1), we found that greater grid-cell–like representations (in addition to higher values of central navigational preference, younger age and male sex) were positively related to spatial memory performance (supplementary text and fig. S6). This result strengthens the hypothesis that EC-specific representations of space guide behavior in humans (*15*, *18*). Nevertheless, this result also seemed paradoxical to us: Given that *APOE*-ε4 reduces grid-cell–like representations and that reduced grid-cell–like representations are associated with impaired spatial memory performance, how can we explain similar performance between both genetic subgroups? Therefore, we hypothesized that there are compensatory mechanisms in risk participants (*19*).

We anticipated hippocampal task-related activity to be a compelling option for a potential compensatory mechanism because the importance of the hippocampus for spatial memory is well established (*20*), and hippocampal activity is altered in *APOE*-ε4 carriers (*21*). Hippocampal task-related activity (contrast of task versus implicit baseline; methods and table S6) was negatively correlated with grid-cell–like representations across all participants (bilateral hippocampus: Pearson's $r = -0.317$, $P = 0.006$; Fig. 2; right hippocampus: $r = -0.292$, $P = 0.011$; left hippocampus: $r = -0.320$, $P = 0.005$). Particularly in the posterior hippocampus, which is especially relevant for spatial navigation [the bilateral posterior third; see (*22*)], this relationship was significantly more pronounced in risk participants than in control participants (risk participants: $r = -0.545$, $P < 0.001$; control participants: $r = -0.064$, $P = 0.707$; difference between correlation coefficients, $z = -2.27$, $P = 0.023$; fig. S7). Because reduced grid-cell–like representations were also correlated with increased task-related activity of the EC and amygdala (fig. S8), we then examined the behavioral relevance of hippocampal task-related activity. Detailed analyses revealed that increased task-related activity, particularly in the left posterior hippocampus, was associated with better spatial memory performance (supplementary text, tables S3 and S7, and fig. S9). In short, increased hippocampal activity could serve as a behaviorally relevant compensatory mechanism for reduced grid-cell–like representations. Nevertheless, increased hippocampal activity may also indicate a broader disruption of medial temporal lobe computations promoting pathological processes [(*23*, *24*); for further discussion, see the supplementary text].

Next, we aimed at understanding the reduction of grid-cell–like representations in risk participants in greater detail. In principle, reduced grid-cell–like representations in fMRI could be due to (i) temporal instability of the putative grid axes across the entire experiment, (ii) spatial instability of the putative grid axes within each half of the experiment, or—similar temporal and spatial stability between genetic subgroups in smaller data segments provided—(iii) a relatively weaker right EC contrast of aligned versus misaligned movements. We sought to disentangle this ambiguity by first calculating one temporal stability and one spatial stability value for each participant (methods; Fig. 3). Temporal stability values differed between genetic subgroups (t_{73} = 2.408, P = 0.019), were positively correlated with grid-cell–like representations (Pearson's r = 0.736, P < 0.001; Fig. 3B), and were also negatively correlated with hippocampal task-related activity (r = −0.311, P = 0.007). Reduced temporal stability values were related to decreased functional connectivity between the right EC and hippocampus, possibly indicating a decoupling of both regions associated with entorhinal dysfunction (r = 0.298, P = 0.009; supplementary text and fig. S10). In contrast, spatial stability values did not differ between genetic subgroups and were not related to the grid-cell–like representations (t_{73} = −0.143, P = 0.887; r = −0.079, P = 0.501; Fig. 3). Finally, to disentangle reduced grid-cell–like representations from reduced temporal stability, we analyzed grid-cell–like representations on shorter data segments (methods). This analysis revealed significant grid-cell–like representations in control participants (t_{36} = 2.708, P = 0.010) but not in risk participants (t_{37} = −0.788, P = 0.436), with a significant difference between both groups (t_{73} = 2.315, P = 0.023; fig. S11), although the corresponding temporal and spatial stability values did not differ between groups (temporal stability: t_{73} = 1.459, P = 0.149; spatial stability: t_{73} = −0.421, P = 0.675). Taken together, this demonstrates that grid-cell–like representations in risk participants were less robust than in control participants (on a shorter time scale) and that the grid orientations of potential grid-cell–like representations were additionally temporally instable in risk participants (on a longer time scale).

Our results (summarized in fig. S12) support the hypothesis that AD involves the dysfunction of entorhinal grid cells. Adults at genetic risk for AD exhibit strongly reduced fMRI representations of grid cells, and reduced grid-cell–like representations are related to impaired spatial memory performance (for a speculative interpretation of the underlying mechanistic basis, see the supplementary text). We also found a reduced preference of risk participants to navigate in the center of a virtual arena. This change in navigational strategy may be interpreted (i) as an attempt to correct errors in the grid code by encounters with environmental boundaries (*25*), (ii) as an uncertainty to rely on entorhinal path integration mechanisms, (iii) as a shift toward a response-based strategy relying on different mountain-wall conjunctive features, or (iv) as a result of inaccurate place fields in the arena center due to impaired grid cell input on place cells (*26*). Moreover, our results offer an explanation for the previously observed hyperactivity of certain brain areas in *APOE*-ε4 carriers (*27*): They may compensate for entorhinal dysfunction. Specifically, our data would be in line with behaviorally relevant compensatory hyperactivity of the hippocampus that could indicate a stronger hippocampus-dependent boundary-based strategy (*28*) or enhanced hippocampal path integration computations (*29*, *30*) to counter impaired entorhinal path integration. Such neuronal hyperactivity could cause partial benefits at a young age (*31*) but may induce further pathological spreading afterward (*24*), including the degradation of place cell firing, which has already been shown in a mouse model of AD (*32*). Thus, the increased hippocampal activation may also reflect an adverse condition. Our results could provide a

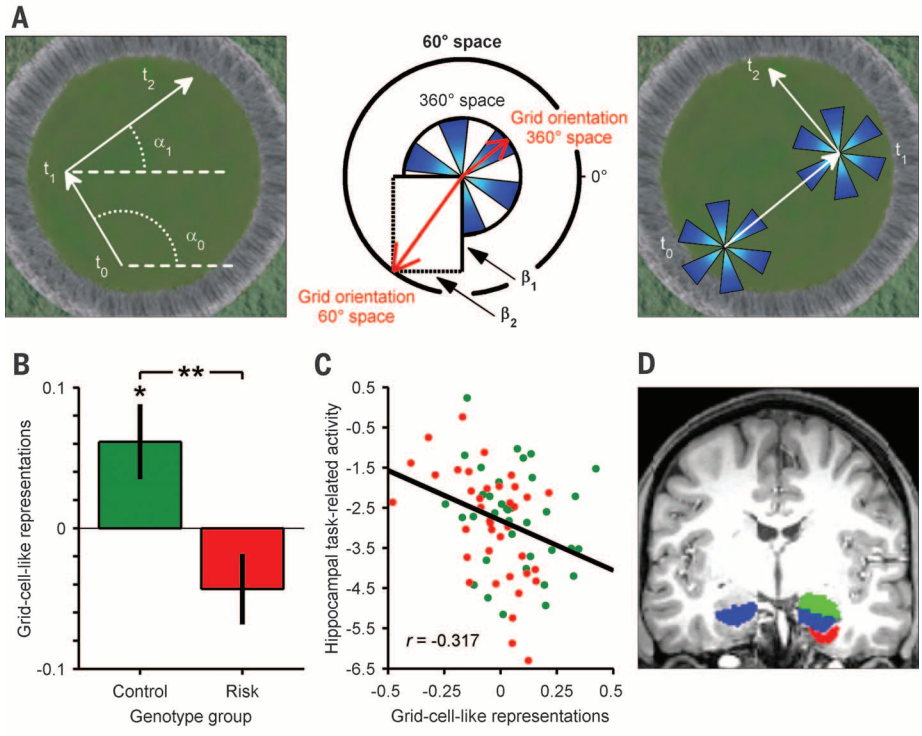

Fig. 2. Grid-cell–like representations and compensatory hippocampal activity. (**A**) Analysis procedure. (Left) The first half of the data was modeled with a general linear model (GLM), including one regressor for movement in the virtual arena. Two parametric modulators model movement direction in 60° space (sixfold rotational symmetry). t, time; α, running angle. (Middle) The putative grid orientation in 60° space is calculated via the β values of these parametric modulators (β_1 and β_2). Dividing by 6 yields the grid orientation in 360° space. Blue areas depict resulting aligned bins. (Right) Fitting a new GLM to the second half of the data allows the contrast of aligned versus misaligned movements to be calculated. (**B**) Grid-cell–like representations in the right entorhinal cortex (EC) are present for control participants but not for risk participants. In fact, grid-cell–like representations are reduced for risk participants as compared to control participants. (**C**) Negative correlation of task-related hippocampal activity with the magnitude of grid-cell–like representations (P = 0.006). (**D**) Exemplary ROIs of one participant, created using Freesurfer (methods). Red, right EC; blue, bilateral hippocampus; green, right amygdala. All bars show mean and SEM across participants. Green dots represent control participants; red dots represent risk participants. Units of all contrasts are parameter estimates. *P < 0.05, **P < 0.01.

Table 1. Multiple regression to predict spatial memory performance (N = 75 participants). Adjusted coefficient of determination (R^2) = 0.170. Multicollinearity was not a concern (all variance inflation factors < 1.214).

Predictor	β	t	P
Grid-cell–like representations	0.237	2.077	0.042
Central navigational preference	0.236	2.130	0.037
Genotype (control/ risk)	0.138	1.179	0.242
Sex (male/female)	−0.282	−2.643	0.010
Age (years)	−0.306	−2.830	0.006

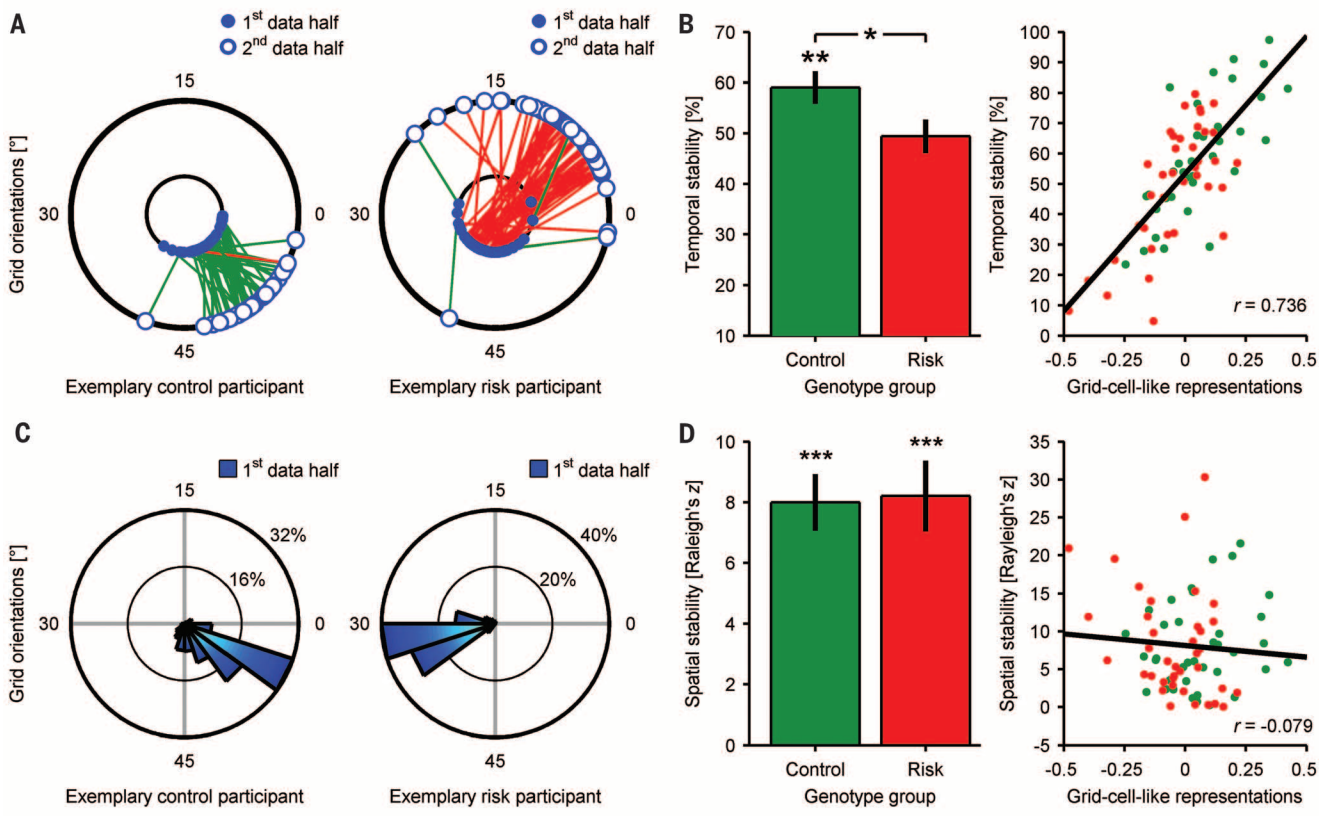

Fig. 3. Stability metrics of grid-cell–like representations. (**A**) Exemplary plots from one participant per group show temporally stable grid orientations (connected by green lines) and temporally instable grid orientations (red lines) of individual voxels, leading to one percentage value per participant ("temporal stability"). The exemplary plot for the risk participant indicates that the voxel-wise grid orientations change between the two halves of the data (lines between circles), but that within each half, the voxel-wise grid orientations are clustered (dots placed on the different circles, see spatial stability). (**B**) Temporal stability values show a reduction in risk participants and are highly correlated with grid-cell–like representations ($P < 0.001$), suggesting temporal instability as a cause of reduced grid-cell–like representations. (**C**) Exemplary plots showing spatially stable grid orientations estimated from the first half of the data (Rayleigh's $z > 11$ for both). (**D**) Contrarily to temporal stability, spatial stability values do not differ between genetic subgroups and are not related to grid-cell–like representations. All bars show mean and SEM across participants, separately for both groups. Green dots represent control participants; red dots represent risk participants. Units of all contrasts are parameter estimates. *$P < 0.05$, **$P < 0.01$, ***$P < 0.001$.

new basic framework for preclinical research on AD and may provide a neurocognitive explanation of spatial disorientation in AD. We emphasize their early occurrence in young adulthood, which may help to determine treatment onset and to establish entorhinal dysfunction as a prognostic marker. The amelioration of entorhinal dysfunction might be a new therapeutic target in the treatment of AD.

REFERENCES AND NOTES

1. H. W. Querfurth, F. M. LaFerla, *N. Engl. J. Med.* **362**, 329–344 (2010).
2. R. A. Sperling, C. R. Jack Jr., P. S. Aisen, *Sci. Transl. Med.* **3**, 111cm33 (2011).
3. E. H. Corder *et al.*, *Science* **261**, 921–923 (1993).
4. C. C. Liu, T. Kanekiyo, H. Xu, G. Bu, *Nat. Rev. Neurol.* **9**, 106–118 (2013).
5. H. Braak, E. Braak, *Acta Neuropathol.* **82**, 239–259 (1991).
6. H. Braak, K. Del Tredici, *Acta Neuropathol.* **121**, 171–181 (2011).
7. E. Ghebremedhin, C. Schultz, E. Braak, H. Braak, *Exp. Neurol.* **153**, 152–155 (1998).
8. T. Hafting, M. Fyhn, S. Molden, M. B. Moser, E. I. Moser, *Nature* **436**, 801–806 (2005).
9. J. Jacobs *et al.*, *Nat. Neurosci.* **16**, 1188–1190 (2013).
10. G. Buzsáki, E. I. Moser, *Nat. Neurosci.* **16**, 130–138 (2013).
11. M. E. Hasselmo, M. P. Brandon, *Neural Plast.* **2008**, 658323 (2008).
12. S. Sreenivasan, I. Fiete, *Nat. Neurosci.* **14**, 1330–1337 (2011).
13. D. Bush, C. Barry, N. Burgess, *Trends Neurosci.* **37**, 136–145 (2014).
14. A. D. Ekstrom *et al.*, *Nature* **425**, 184–188 (2003).
15. C. F. Doeller, C. Barry, N. Burgess, *Nature* **463**, 657–661 (2010).
16. Materials and methods are available as supplementary materials on *Science* Online.
17. F. Berteau-Pavy, B. Park, J. Raber, *Neuroscience* **147**, 6–17 (2007).
18. M. J. Chadwick, A. E. Jolly, D. P. Amos, D. Hassabis, H. J. Spiers, *Curr. Biol.* **25**, 87–92 (2015).
19. S. Y. Bookheimer *et al.*, *N. Engl. J. Med.* **343**, 450–456 (2000).
20. B. A. Strange, M. P. Witter, E. S. Lein, E. I. Moser, *Nat. Rev. Neurosci.* **15**, 655–669 (2014).
21. N. Filippini *et al.*, *Proc. Natl. Acad. Sci. U.S.A.* **106**, 7209–7214 (2009).
22. M. S. Fanselow, H. W. Dong, *Neuron* **65**, 7–19 (2010).
23. A. Bakker *et al.*, *Neuron* **74**, 467–474 (2012).
24. A. W. Bero *et al.*, *Nat. Neurosci.* **14**, 750–756 (2011).
25. K. Hardcastle, S. Ganguli, L. M. Giocomo, *Neuron* **86**, 827–839 (2015).
26. L. Muessig, J. Hauser, T. J. Wills, F. Cacucci, *Neuron* **86**, 1167–1173 (2015).
27. A. J. Trachtenberg, N. Filippini, C. E. Mackay, *Neurobiol. Aging* **33**, 323–334 (2012).
28. C. F. Doeller, J. A. King, N. Burgess, *Proc. Natl. Acad. Sci. U.S.A.* **105**, 5915–5920 (2008).
29. T. Wolbers, J. M. Wiener, H. A. Mallot, C. Büchel, *J. Neurosci.* **27**, 9408–9416 (2007).
30. K. R. Sherrill *et al.*, *J. Neurosci.* **33**, 19304–19313 (2013).
31. C. R. Mondadori *et al.*, *Cereb. Cortex* **17**, 1934–1947 (2007).
32. F. Cacucci, M. Yi, T. J. Wills, P. Chapman, J. O'Keefe, *Proc. Natl. Acad. Sci. U.S.A.* **105**, 7863–7868 (2008).

ACKNOWLEDGMENTS

The authors thank H. Boecker, V. Heise, W. Huijbers, T. Reber, and S. Remy for comments on the manuscript and A. Rühling and Y. Sagik for their help with fMRI scanning. We also thank all of the participants for their participation in this study. L.K. was supported by a Bonfor dissertation stipend of the Medical Faculty of the University of Bonn and a stipend of the German National Academic Foundation (Studienstiftung des deutschen Volkes). C.M. is funded by a Heisenberg grant awarded to him by the German Research Foundation (DFG, MO 2363/3-1). P.C.M.F. was supported by a stipend of the Konrad Adenauer Foundation (Konrad-Adenauer-Stiftung). C.F.D. and T.N.S. are supported by the European Research Council (grant ERC-StG 261177) and the Netherlands Organisation for Scientific Research (grant NWO-Vidi 452-12-009). N.A. received DFG funding from Emmy Noether grant AX82/2 and together with J.F. via the Sonderforschungsbereich 1089. The authors declare no conflicts of interest. All raw data are archived at the German Center for Neurodegenerative Diseases (DZNE), Bonn.

SUPPLEMENTARY MATERIALS

www.sciencemag.org/content/350/6259/430/suppl/DC1
Materials and Methods
Supplementary Text
Figs. S1 to S12
Tables S1 to S7
References (*33*–*62*)

17 June 2015; accepted 23 September 2015
10.1126/science.aac8128

Science
AAAS

Reduced grid-cell–like representations in adults at genetic risk for Alzheimer's disease

Lukas Kunz *et al.*

Science **350**, 430 (2015);
DOI: 10.1126/science.aac8128